REPORT DOCUMENTATION PAGE

Public reporting burden for this collection of information is estimated to average 1 hour per response, including the time for reviewing instructions, searching existing data sources, gathering and maintaining the data needed, and reviewing the collection of information. Send comments regarding this burden estimate or any other aspect of this collection of information, including suggestions for reducing this burden, to Washington Headquarters Services, Directorate for Information Operations and Reports, 1215 Jefferson Davis Highway, Suite 1204, Arlington, VA 22202-4302, and to the Office of Information and Regulatory Affairs, Office of Management and Budget, Washington, DC 20503.

1. AGENCY USE ONLY (Leave blank)	2. REPORT DATE Report Date 3/28/95	3. REPORT TYPE AND DATES COVERED Technical Report (Final)

4. TITLE AND SUBTITLE

Progress Report on Velocity, Vorticity and Density Observations in the Ocean Boundary Layer

5. FUNDING NUMBERS

ONR Grant N00014-93-1-0408

6. AUTHOR(S)

Thomas B. Sanford

7. PERFORMING ORGANIZATION NAME(S) AND ADDRESS(ES)

Applied Physics Laboratory
University of Washington
1013 NE 40th Street
Seattle, WA 98105-6698

8. PERFORMING ORGANIZATION REPORT NUMBER

None

9. SPONSORING / MONITORING AGENCY NAME(S) AND ADDRESS(ES)

Office of Naval Research
Code 1122SS
800 N. Quincy St.
Arlington, VA 22217-5000

10. SPONSORING / MONITORING AGENCY REPORT NUMBER

None

11. SUPPLEMENTARY NOTES

12a. DISTRIBUTION / AVAILABILITY STATEMENT

Distribution Statement

DISTRIBUTION STATEMENT A

Approved for public release;
Distribution Unlimited

12b. DISTRIBUTION CODE

13. ABSTRACT (Maximum 200 words)

The Vorticity Meter has been assembled, merged with ancillary sensors and operated from a new tow body. The system consists of three components: the VM sensor, support electronics and ancillary sensors. Some redesign had to be undertaken to overcome problems and unforeseen requirements, such as accepting additional sensors that were not earlier included.

19950925 133

14. SUBJECT TERMS

Subject Terms

15. NUMBER OF PAGES

Pages

16. PRICE CODE

17. SECURITY CLASSIFICATION OF REPORT	18. SECURITY CLASSIFICATION OF THIS PAGE	19. SECURITY CLASSIFICATION OF ABSTRACT	20. LIMITATION OF ABSTRACT
Unclassified	Unclassified	Unclassified	

Progress Report on Velocity, Vorticity and Density
Observations in the Ocean Boundary Layer
by Thomas B. Sanford, APL-UW

I. Results from Current Research

- *Completion of Gulf of Cadiz Research*

This year was the culmination of this project. Numerous publications appeared or are in press. Table I reviews the current status of project supported publications resulting from this project. There are some small projects underway, mainly with European colleagues (e.g., Rolf Käse), which were formulated as a consequence of mutual interests in instabilities and Meddy formation. No manuscripts have resulted from this collaboration as of yet.

- *Vorticity Meter (VM) Instrumentation*

The new VM sensor was developed under N87 support. This program was terminated before the sensors and system were completed. APL-UW fees and early ONR contributions permitted the construction and/or evaluation of the sensor. Under ONR support a non-metallic tow body was developed for operating the VM and ancillary sensors in the ocean. Two field experiments were undertaken to study velocity and vorticity in local tidal channels.

Two technical reports have been written on the design and observations of the VM. A comprehensive report is under security review, which details the theory of operation, design and field measurements of the Vorticity Meter. A second report is being prepared on the first scientific observations with the VM in a turbulent tidal channel. Results for these measurements are presented later in this section.

The Vorticity Meter has been assembled, merged with ancillary sensors and operated from a new tow body. The system consists of three components: the VM sensor, support electronics and ancillary sensors. Some redesign had to be undertaken to overcome problems and unforeseen requirements, such as accepting additional sensors that were not included in the N87 effort.

A. Sensor

The latest Vorticity Meter uses a strong permanent magnet and pre-amps and A/Ds in the sensor head. The specifications are:
- Electrodes: silver-silver chloride: APL-UW manufacture
- Preamplifiers: AMP-01; IC differential instrumentation amplifiers, 4 channels, X500
- Digitizers: Analog Devices AD7703, 20-bit, 10-Hz, 4 individual channels
- Magnet: NdFeB (37A) with magnetic field of .065T at 2.5" above the sensor
- Body: Lexan with PVC flow splitting plate to form regular boundary layer
- Sensor tubes: Alumina ceramic, 0.1" OD, agar filled, ends 2.5" above splitter plate
- Connectors: Impulse Enterprise, LPBH-3 (3-pin power), LPBH-9 (9-pin digital)

B. Electronics

The main electronics, housed in a separate plastic cylinder, provide clock signals and power to the sensor head, storage and transmission of data, and ancillary measurement, such as pitch, pressure, etc. The auxiliary channels and their uses are:
- Time: time since last reset
- Pitch: to rotate velocity into vertical and horizontal components
- Pitch rate: to correct apparent vorticity for sensor rotation rate
- Pressure: to measure sensor depth

The measurements are controlled, processed and stored by the Onset Computer model TT-7 microcomputer that has a 20 Mbyte disk. The channels are stored at 20-Hz rate onboard, while 1-Hz averages are sent to the deck unit via RS-485. A custom program was written in C for the TT-7 microprocessor. The C code was passed through a cross compiler to form the 680x0 object

Table 1: Publications supported by ONR in FY94

Gulf of Cadiz: Ampere Seamount Studies

Kunze, E. and T. B. Sanford, 1993: Submesoscale Dynamics near a Seamount: I. Measurements of Ertel vorticity. *J. Phys. Oceanogr.,* **23,** 2567-2588.

Kunze, E., 1993: Submesoscale Dynamics near a Seamount: II. The partition of energy between internal waves and geostrophy. *J. Phys. Oceanogr.,* **23,** 2589-2601.

Gulf of Cadiz: Meddy Studies

Prater, M. D. and T. B. Sanford, 1994: A Meddy off Cape St. Vincent, Portugal: I. Description. *J. Phys. Oceanogr.,* **24,** 1572-1586.

Prater, M. D., 1994: A Meddy off Cape St. Vincent, Portugal: II. Origin and Generation. *J. Phys. Oceanogr.,* **24,** (in press).

Gulf of Cadiz: Med Outflow Studies

Johnson, G. C., T. B. Sanford, and M. O. Baringer, 1994b: Stress on the Mediterranean outflow plume: Part 1. Velocity and water property measurements. *J. Phys. Oceanogr.,* (in press).

Johnson, G. C., R. G. Lueck, and T. B. Sanford, 1994a: Stress on the Mediterranean outflow plume: Part 2. Turbulent dissipation and shear measurements. *J. Phys. Oceanogr.,* (in press).

Other outflow studies:

Johnson, G. C. and D. R. Ohlsen, 1994: Frictional rotating channel exchange and ocean outflows. *J. Phys. Oceanogr.,* **24,** 66-78.

Other studies:

Price, J. F., T. B. Sanford and G. Z. Forristall, 1993: Observations and simulations of the forced stage response to moving hurricanes. *J. Phys. Oceanogr.,* **24,** 233-260.

Sanford, T. B., M. S. Horgan and N. A. Bond, 1994: Upper ocean velocities and shears in response to extreme winds. *J. Phys. Oceanogr.,* (in preparation).

Sanford, T. B., J. A. Carlson, and M. D. Prater, 1994: An Electromagnetic Vorticity Meter. *APL-UW TR,* Applied Physics Laboratory, University of Washington, Seattle, WA, (in preparation).

Sanford, T. B., J. A. Carlson, J. H. Dunlap, and R. A. Leathers, 1994: Vorticity in Pickering Passage Tidal Channel: Cruise Report and Preliminary Results. *APL-UW TR,* Applied Physics Laboratory, University of Washington, Seattle, WA, (in preparation).

code which was burned into the EEPROM resident on the TT-7 microprocessor.

After assembly of the sensor and support electronics, the system was evaluated on the bench and in the salt water tank in our lab. It was towed and rotated in the tank to check the calibrations which were compared with theoretical values.

C. Ancillary sensor and systems

Sea-Bird Electronics temperature and electrical conductivity sensors are plugged directly into the main electronics providing 20-Hz measurements and real-time, 1-Hz property information.

A Sea-Bird Electronics, Inc. Seacat CTD is installed on the tow body. It is a self-contained unit, without connection to the VM electronics. The Seacat is capable of measuring temperature, electrical conductivity and pressure at 2-Hz with accuracies of ± 0.005 °C, ± 0.0005 S m^{-1} and $\pm$ 0.1 dbar, respectively. For the Pickering Passage experiment, the data were downloaded to the lab computer after the package was recovered. These measurements are redundant to those collected by the individual sensors connected to the system electronics.

Altitude or height above the bottom is measured by a Datasonics, Model PSA-900 altimeter borrowed from Mike Gregg's project. This device is mounted 24 cm (9.5") above the bottom of the tow body. It had an accuracy of $\pm$ .75 cm. It failed to register correctly when less than 0.86 m or more than 30 m off the bottom. The altimeter is electrically connected to the VM electronics, which merged the altitude with the vorticity data, stored the observations and transmitted 1-s averages to the deck. This device proved to be very valuable in allowing us to approach but not to strike the bottom while profiling.

A KVH magnetic compass was installed in the tail of the tow body to provide heading information. It was far enough from the VM magnets to register direction within manufacturer's specifications.

D. Computer and Deck Equipment

The data acquisition system consists of a Mac IIfx computer with a large color monitor, laserwriter and data storage devices. The interface with the underwater unit is via a Black Box RS-486 to 232 converter. The equipment was scrounged from existing hardware; no support was available for a proper data acquisition system. This placed some restrictions on performance and real-time processing because the available equipment was, by and large, older and slower than new versions.

Software was written to cope with the facilities of the available equipment and provide real-time display of the VM observations. The software was written in C and compiled for the Mac using the Think C compiler. The data acquisition program accepted data at 57.6 kbaud, displayed multiple channels on the color monitor and archived the observations to a 300 MB hard disk.

E. Winch, cable and rigging

Our Sea Mac 3510 EAHL winch with 200 m of 24-conductor cable was used to raise and lower the VM on the tow body. The Sea Mac, purchased under prior VM support from Ken Ferer, is a electro-hydraulic winch with variable speed powered by a 10-HP, 230-VAC motor driving a variable displacement hydraulic pump. Haul-in and payout speeds are continuously variable via a joystick control. Maximum rates of 100 fpm can be achieved under light loading. Maximum pull is 5000 lbs. It is fitted with an IEC Corp. slipring assembly (IEL-BX-24) with 24 contact pairs.
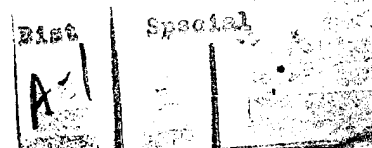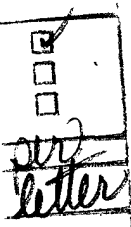
The electro-mechanical cable contains 24 conductors with Kevlar strength member with a polyurethane jacket and is not faired. It was terminated with a Seacon XCL-24-CCP underwater connector manufactured by Brantner & Associates. The attachment of the cable to the tow body was with a Chinese finger type grip. A 12" block was hung from the frame overhanging the diver platform on the stern of APL's Utility Boat (UBoat).

F. Tow body and bottom lander

This vehicle was built under ONR support for providing a stable, flow-oriented platform for VM observations. A design requirement was that the tow body produce neither electric nor magnetic interference. An electromagnetically quiet vehicle was desired to eliminate confounding effects, such as electrical corrosion currents. The tow body was made from PVC and granite. The former provided the structure for supporting two VM sensors and all ancillary systems. The latter provided dead-weight for vehicle stability and eliminated possible corrosion currents from metallic weights. The tow body had mounts for two VMs, one on each side of the body pointing horizontally or with one pointing vertically downward under the body. It was tested in Lake Washington at various speeds with special vibration and attitude sensors for evaluating its mechanical behavior. Its performance was very acceptable.

The tow body and placements of sensors are shown in Fig. 1. It weighs about 207 kg (675 lbs) in air and 216 kg in water without VM and other sensors. It can be towed at speeds up to 5 knots and at depths under 300 m.

A wooden frame, called the bottom lander, was built to support the tow body at a height of 1 m above the bottom. It was not deployed during the experiment because the tow body was very stable in the flow and the need for using the lander was not necessary.

• *Studies of BBL Vorticity and Turbulent Properties in Tidal Channels*

A set of criteria was developed to locate and select sites for experiments. We sought to satisfy all or most of the following:
  • Used in prior BBL observations and published results
  • Known to exhibit unstratified BBL during strong tidal flow
  • Uniform bottom depths for many BBL thicknesses upstream: > 500 m
  • Reasonable, not extreme tidal currents: $U < 1 \text{ m s}^{-1}$
  • Protected location, suitable for foul weather operations
  • Near support services: marina, shore power, accommodations
  • Within 1-day transit for APL's Utility Boat.

A. Pickering Passage

Sternberg (1968) occupied a number of BBL sites in the Puget Sound. He reported a uniform BBL in the Pickering Passage, a channel between Hartstene Island and mainland Washington (Fig. 2). Tidal currents are about 1 knot. This narrow channel has N-S and E-W reaches, permitting a choice of sites depending on wind and wave conditions. Jarrell Cove State Park and the nearby Marina provided mooring and shore power just off the northern reach of Pickering Passage. The town of Shelton, about half an hour away by car, provided accommodations. The transit for the UBoat is about 8 hours.

In order to reduce the UBoat's motion, it was secured with several anchors. The strategy was to deploy anchors so the vessel could be positioned at a slight angle to the wind and current. That is, the intent was to crab into the current to maintain large tensions on the multi-point anchors. The boat's bow anchor was deployed and set. Then a second anchor was carried out
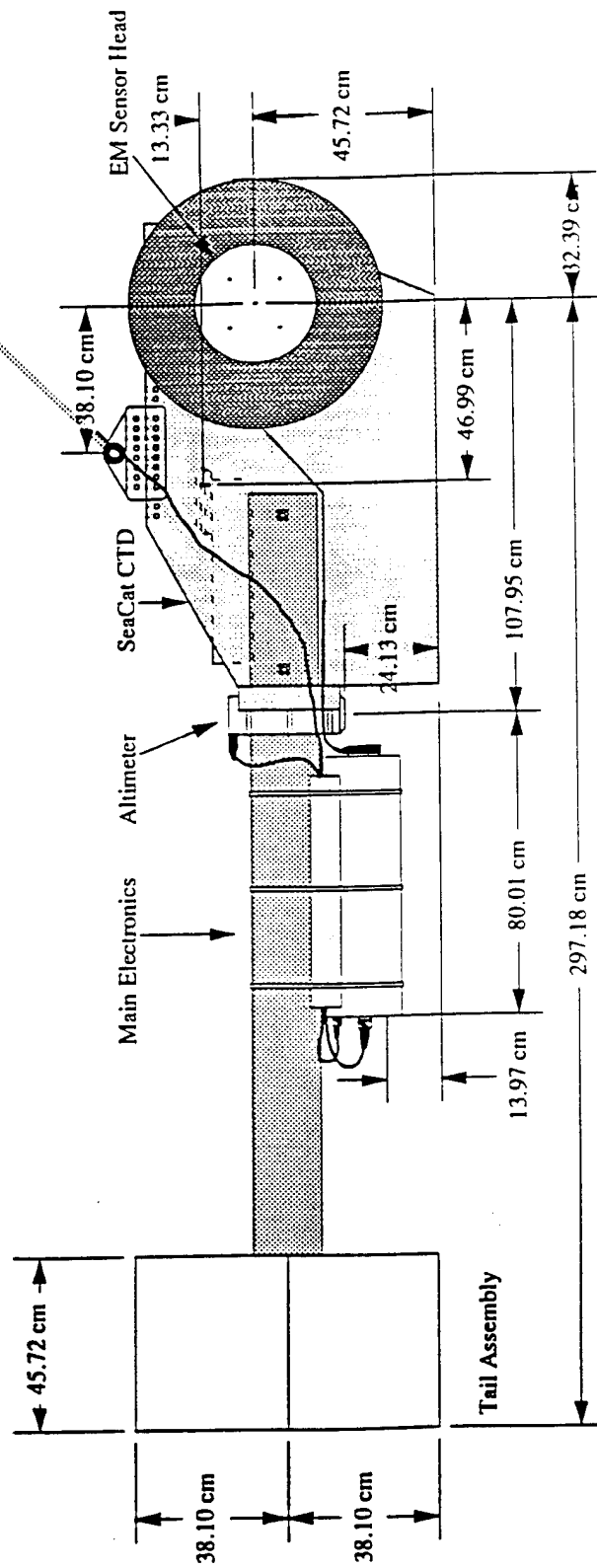
VM Tow Body

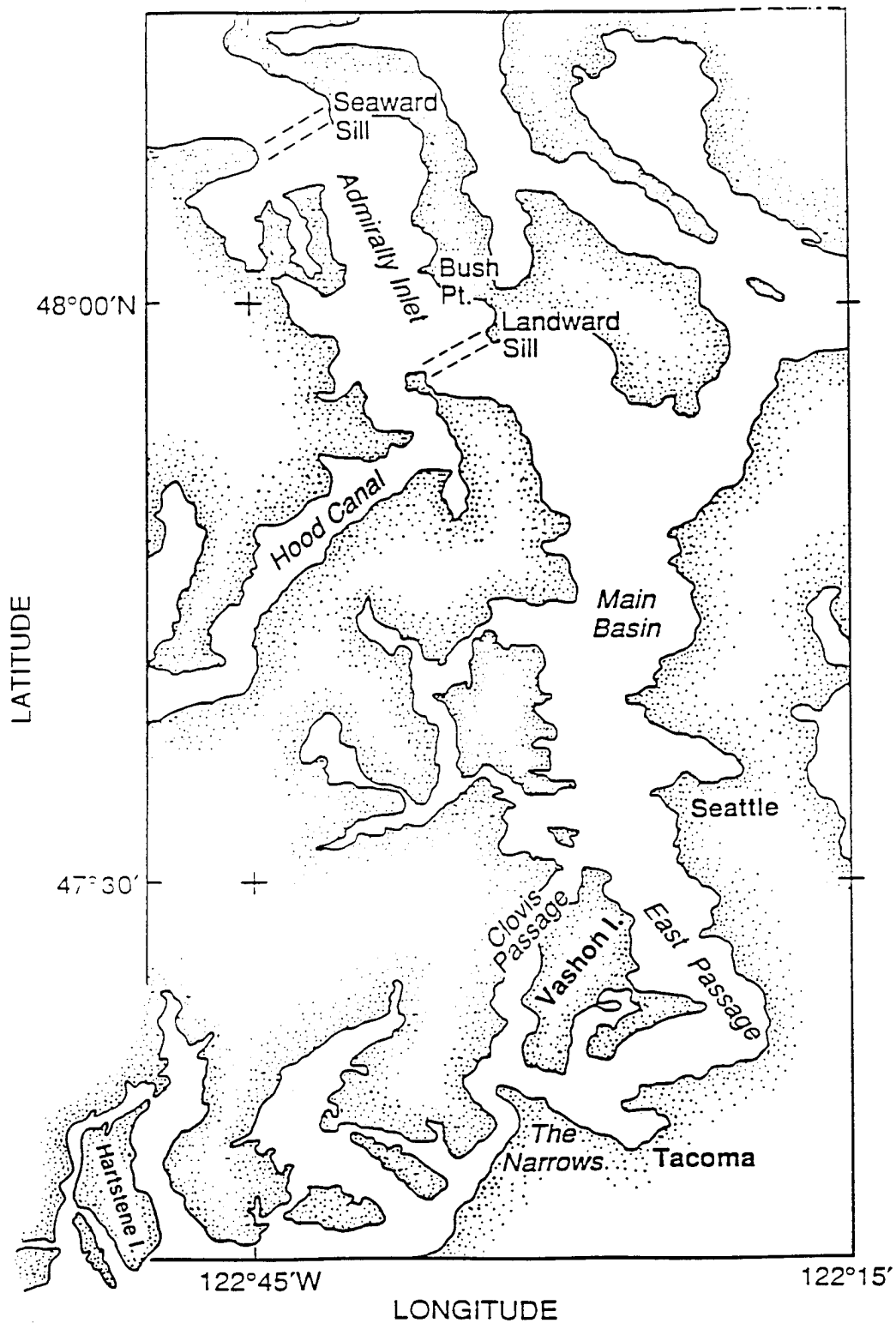Figure 1. Schematic diagram of VM Tow Body.

Figure 2. Chart of South Puget Sound. Pickering Passage, shown
in the lower left hand corner, surrounds Hartstene
Island.

using the Zodiac semirigid boat and deployed off the stern quarter. This was done before the tidal current was very strong. We chose to point the boat into the wind, regardless of the direction of the current, because the wind was often quite strong. This orientation was also good for the strong ebb current, which we were studying. As the current increased, the anchor lines were adjusted to provide the desired angle of attack and stability.

On 30 November, the plan was to use one or both VM sensors and evaluate their performance in the BBL. At this time, there were two small high tides followed by a late evening lower low tide. The best measurements were made late in the evening as the ebb was running strongly.

The location for the second day, 1 December 1993, was about 1.5 km north of the Hartstene Bridge, near where Sternberg (1968) conducted his observations. A depth survey revealed more bottom relief than expected, especially along the channel. A site was finally chosen that was gently shoaling to the north but lacked relief greater than 1 m. Three anchors were deployed off the bow, port quarter and starboard quarter. Once the ebb was running, the boat became relatively stable and good measurements were obtained.

For the third day of measurements, the boat was anchored in the north portion of the channel, not far from the site occupied on the first day. An extensive bottom depth survey was conducted along the majority of this channel. Again rather a lot of bottom relief was observed. The flattest region was selected, and the boat was anchored with the bow and port quarter anchors. The wind was strong and off the port bow once we were anchored. The current and wind combined to set the boat against the anchor lines in the intended fashion.

B. Description of experiment and observations

The plan was to slowly raise and lower the VM to obtain vertical profiles of velocity, vorticity and water properties. Besides the VM, an altimeter and a CTD were installed on the tow body. The VM and altimeter provided 1-s averages in real-time up the cable to the deck equipment. This plan supported performance evaluations and scientific observations. For example, the rate of change of altitude can verify the accuracy of the measurement of the vertical component of velocity. A wooden pedestal, the bottom lander, was built to permit the tow body to rest on the bottom with the VM sensor exactly at 1-m altitude.

C. Processing and performance evaluations

The observations toward the end of 30 November will be used for analysis. This record is denoted nov30c with parts 1 and 2. nov30c2 will be used for most of the analyses.

1. Vorticity Meter

The processing of VM data is discussed in detail in the two technical reports dealing with the VM design and the Pickering Passage observations. It is most appropriate here to present some basic calibration and quality checks for the observations.

a. Height off the bottom

Altitude and pressure were measured. In this experiment, pressure can be equated to depth to within an error of about 1%. Thus, the sum of altitude and pressure should be the water depth. This summation is shown in Fig. 3 where it is clear that the pressure measurement (from the CTD) has a hesitation not seen in the altimeter readings.

b. Velocity

i. Mean velocity: A good check on the velocity measurement is to compare the vertical velocity with rate of change of altitude. Figure 4 shows an example during several vertical
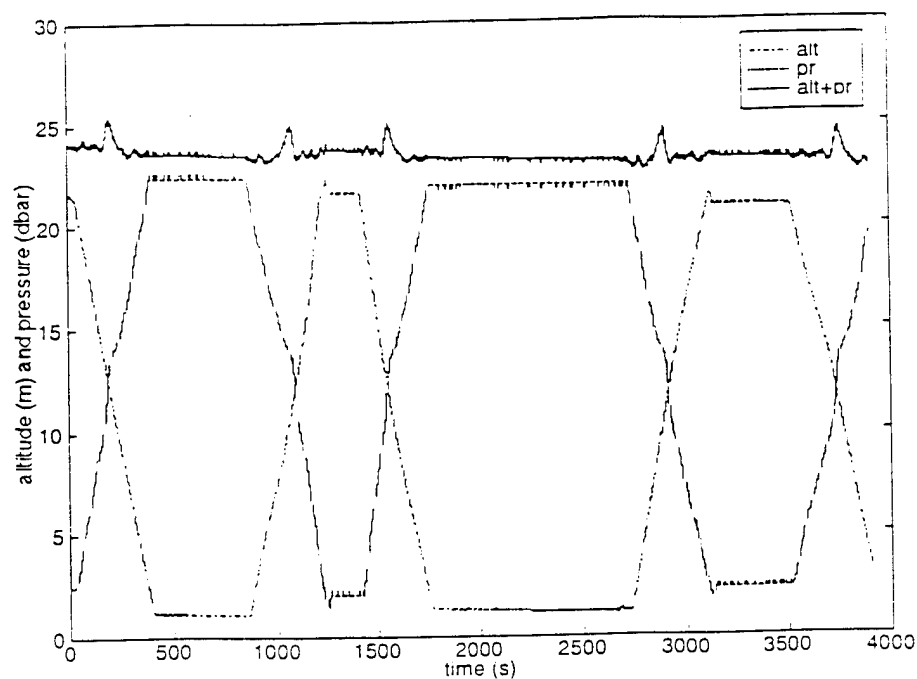
Figure 3. Altitude, Seacat pressure, and their sum. The pressure sensor shows a hesitation near 12 dbar.
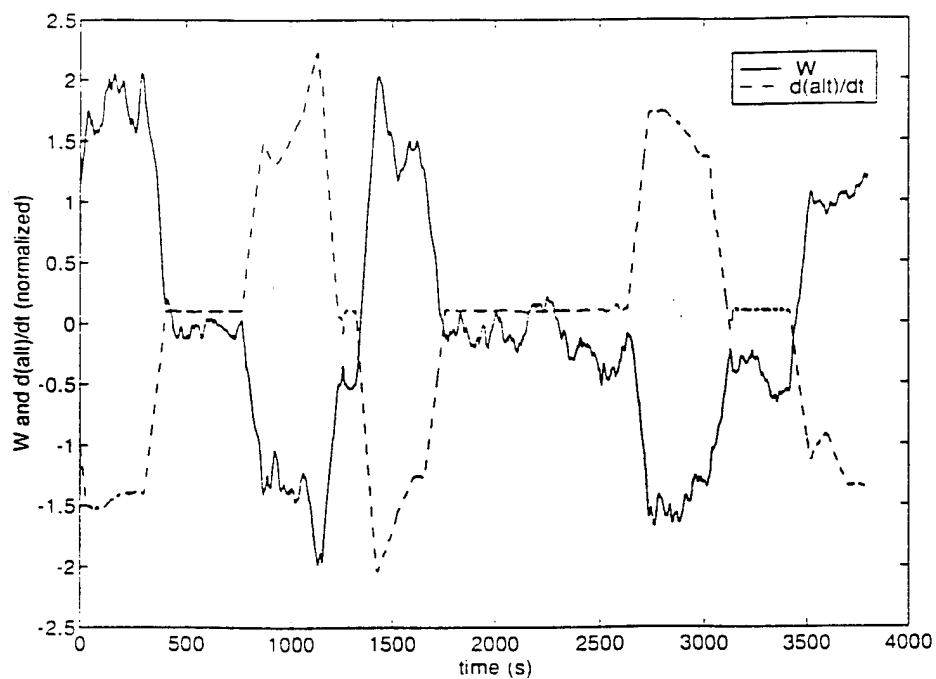

Figure 4. Comparison of vertical velocity (W) and time rate of change of altitude. Values filtered with 100 s boxcar.

traverses of the VM. The corresponding scatter diagram is Fig. 5. During a stretch when VM is not being winched up or down, the correlation between w and pitch is negative with a lag of about 10 s. That is, a positive w is seen to result in a pitch down, a behavior consistent with the large drag on the tail.

Another good check is to determine if w is zero in a long term mean for flow over a long, horizontal bottom and for an 8-minute interval at a height of 1 m $\overline{w} < 0.001$ m s^{-1}.

Another useful check is to show that the time-mean horizontal velocity decreases toward the bottom. Figure 6 shows the mean u profile over for the bottom 20 m of the water column. The lowest bin is 0.5 wide centered at 0.97 m above the bottom and shows a current of 0.38 m s^{-1}.

    ii. Fluctuating velocity: A property of a turbulent BBL is a vertical flux of horizontal momentum due to bottom friction. This is exhibited as a negative correlation between u and w, denoted as $u'w'$. Figure 7 shows the correlation between u' and w' which is large and negative at zero lag. There is much variability to $u'w'/q^2$ as shown in Fig. 8 at time scales of 100-200 s ($q^2 = u'^2 + w'^2$). The character of this statistic is typical of turbulent boundary flow. Much variability is exhibited, but the mean value is clearly negative. Incidentally, the mean value is about the same as that reported in prior BBL studies.

    b. Vorticity

      i. Shrouded sensor observations: The VM cannot distinguish between water vorticity and sensor rotation. Thus, a pitchrate (angular rate) sensor is included to correct the rotation of the sensor. A test of this scheme was to place a large, sea-water filled shroud over the VM sensor. The enclosed water was an inertial mass and tended not to rotate with the VM sensor. Even though the sensor rotated, there was not enough time and drag to produce significant rotation of the trapped water. Some artificial rotations were applied during each VM deployment. A comparison of vorticity and 2 x pitchrate is shown in Fig. 9 while the tow body was yanked about (by grasping on the tow cable between the winch and block and pulling down rapidly). The yanking, done during record nov30c1, was probably too vigorous and less energetic; more typical natural body motions should be applied in the future.

      ii. Vorticity versus mean vertical shear: The detrended record retains the vertical variation of vorticity and can be compared with the mean vertical shear. Figure 10 compares the vertical shear during the multiple traverses of the water column and the corresponding mean, detrended vorticity. For this comparison the data were binned into 5-m wide bins, and mean spanwise vorticity (vorAadt) has been set equal to zero at 15 m where the mean vertical shear is zero. This figure shows that the detrended vorticity and the mean vertical shear are about equal. This near equality of the two versions of vertical shear (or horizontal vorticity) is encouraging.

D. Scientific Analyses and Interpretations

1. Overview of observations

As indicated earlier the data chosen to study were from the file denoted nov30c. The 1-Hz data consist of two segments, called one and two, sized to be processed on a Mac laptop.

2. Stratification, shear and Richardson numbers:

Figure 11 shows the vertical stratification. It should be noted that the range of density variation is less than .01 sigma-t ($\delta\rho/\rho = 10^{-5}$). The stratification below 15 m above bottom (m.a.b.) corresponds to a B-V frequency of 1.9×10^{-3}s^{-1}. This is small stratification, hardly able to provide a restoring force to vertical motion. The Richardson number (i.e., $Ri = N^2 / U_z^2$) is 0.013, well below the value of 0.25 commonly used to indicate the initiation of vigorous vertical
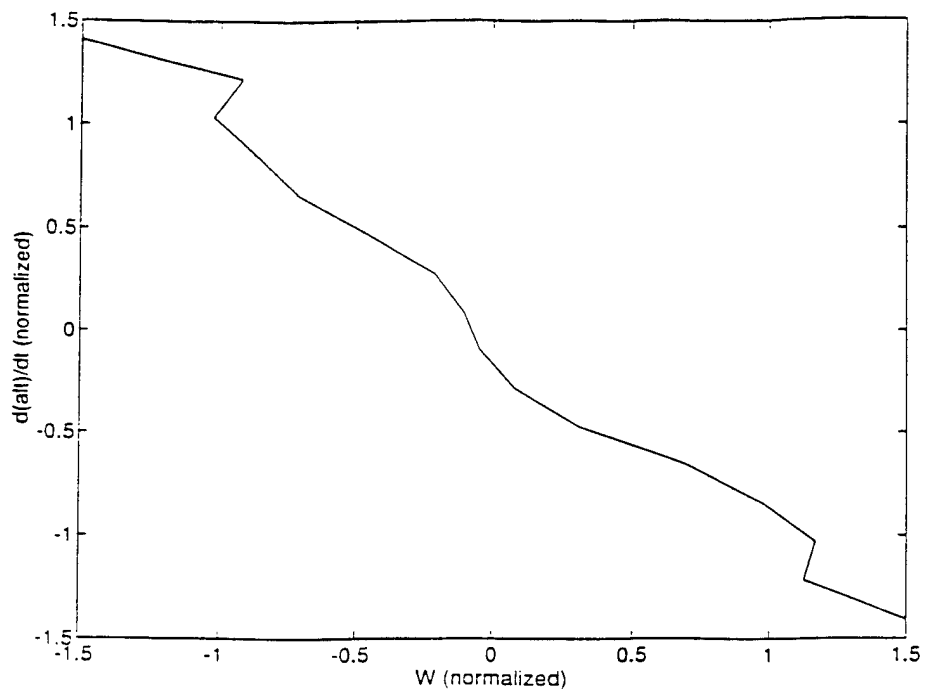
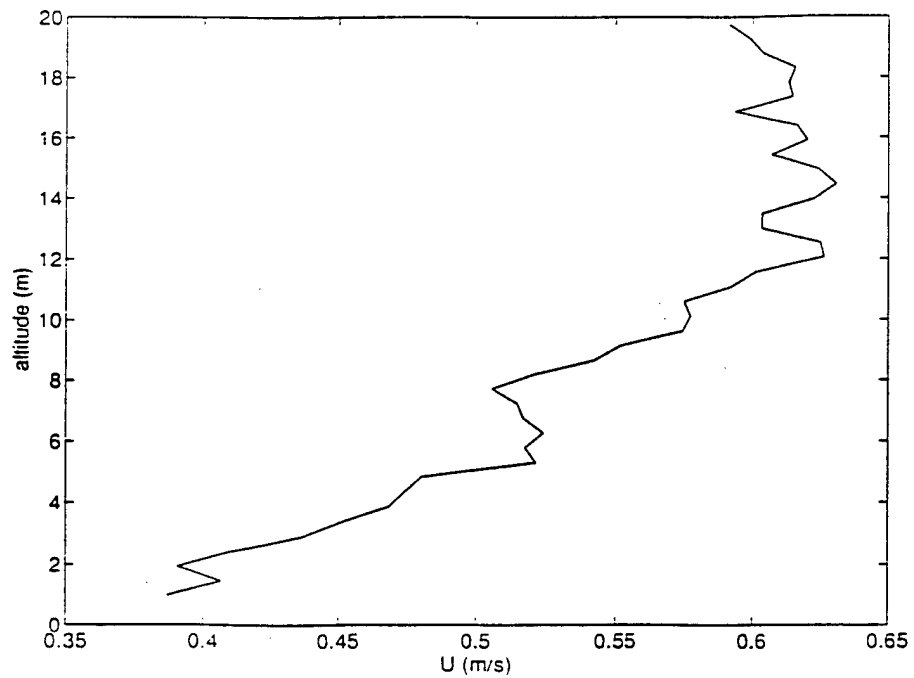Figure 5. Scatter diagram of W and time derivative of altitude.

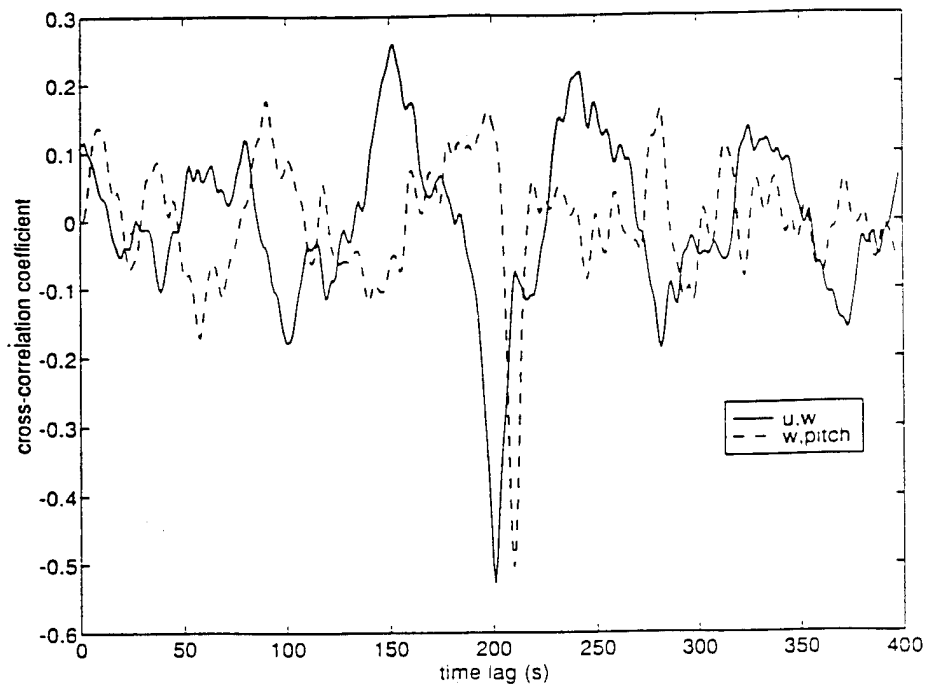Figure 6. Horizontal velocity vs. altitude, binned every 0.5 m.

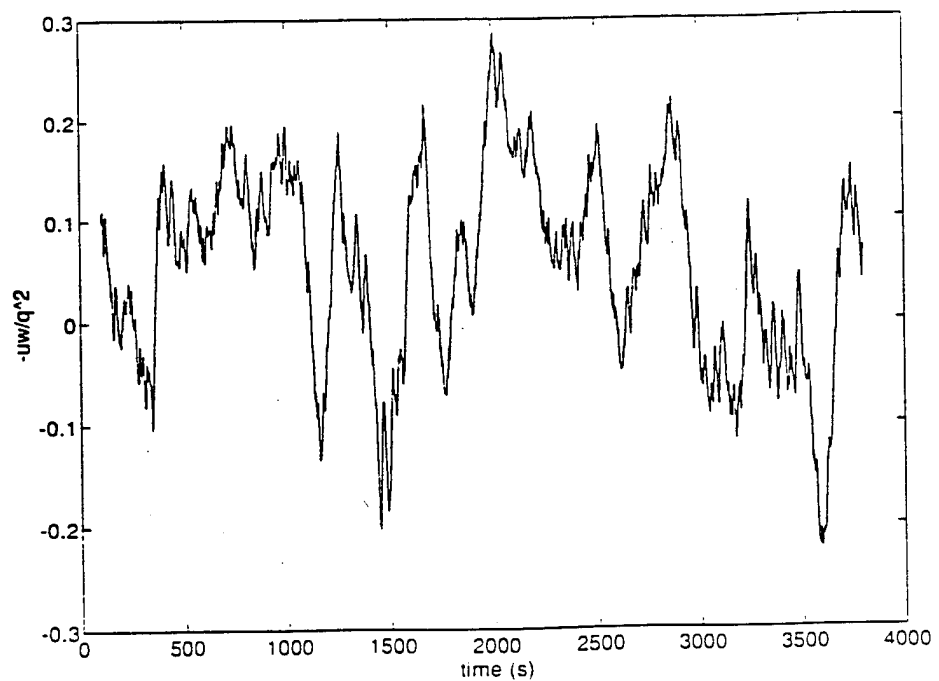Figure 7. Cross-correlations between u and w and between w and pitch.

Figure 8. Time series of - $\overline{uw}/q^2$, averaged with 100s boxcar. Here, $q^2=u^2+w^2$, because v^2 was not measured.
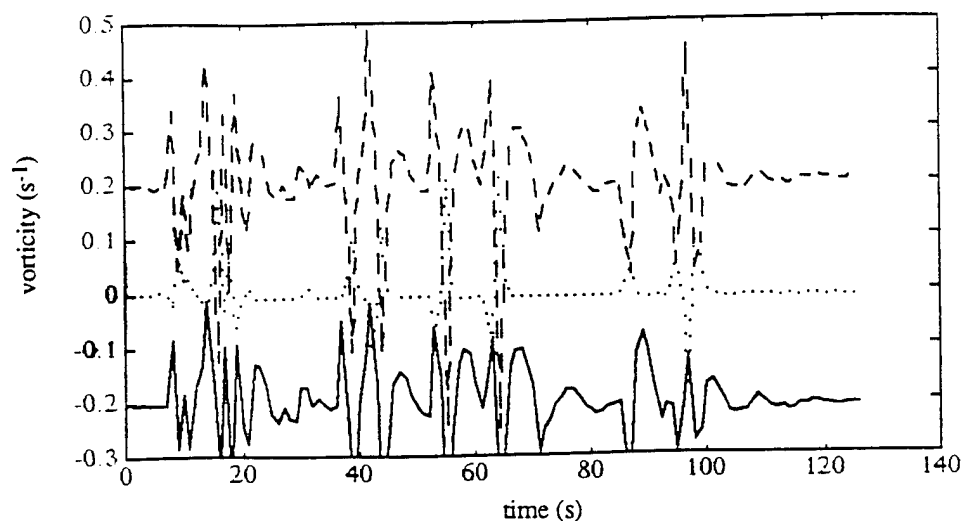
Figure 9. Vorticity, with and without pitch rate correction during period when VM cable was yanked. Lines are offset to avoid overlap. Solid line is measured vorticity $-0.2s^{-1}$; dashed line is 2* pitch rate $+0.2s^{-1}$; dotted line is measured vorticity -2* pitch rate.
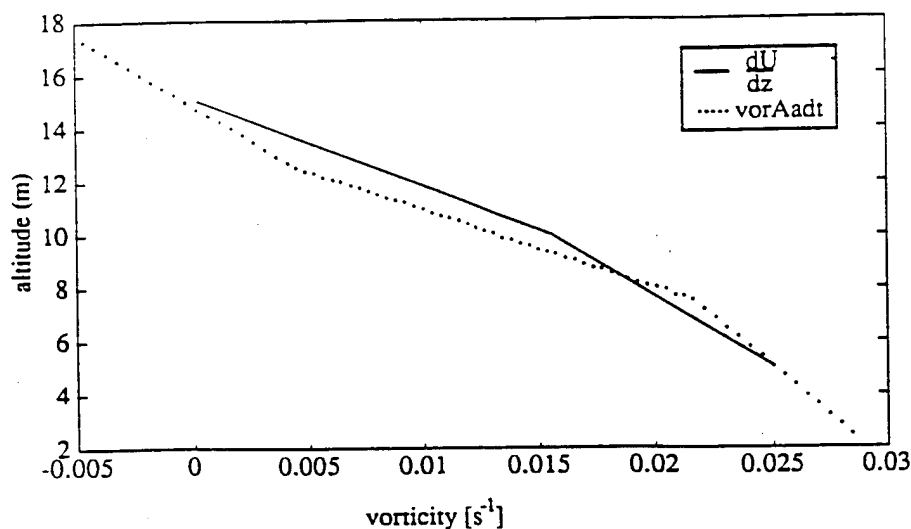

Figure 10. Comparison of the vertical shear and mean (detrended) vorticity. The mean vorticity has been set to zero at 15 m. The agreement in the variation of these quantities with depth is an important validation of the instrument.
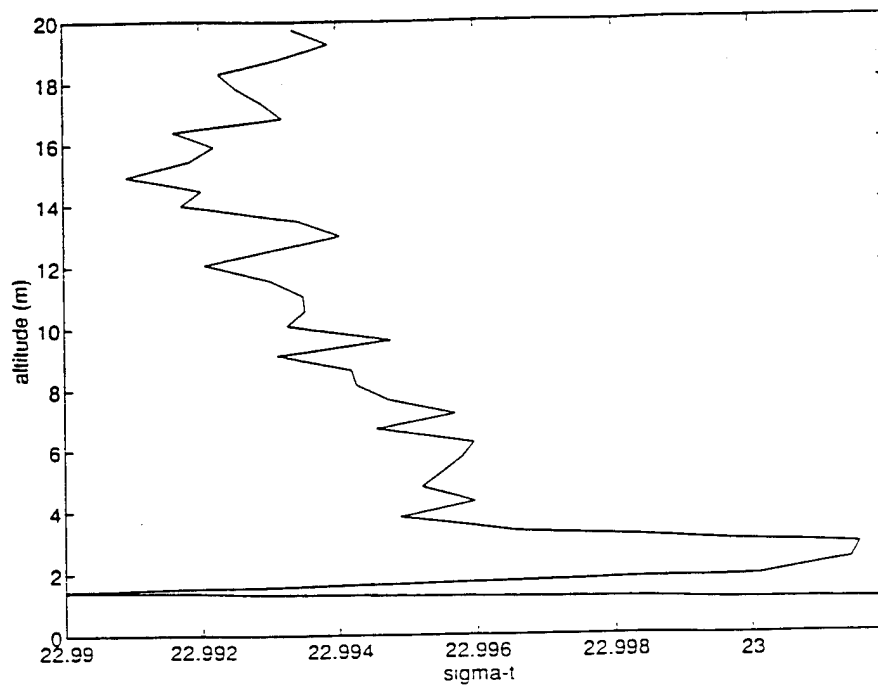
Figure 11. Sigma-t vs. altitude. Note that even the prominent variations amount to density changes of less than 0.01 sigma-t.
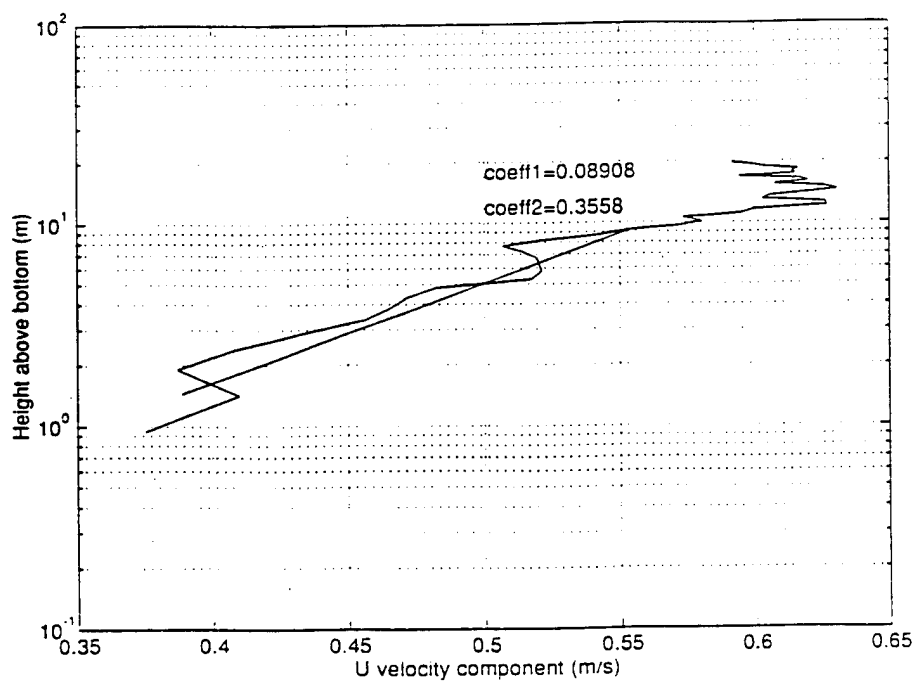

Figure 12. Mean horizontal velocity vs. altitude, in 0.5 m bins.

mixing. The overall stratification is weak enough that homogeneous turbulence is assumed present.

3. Reynolds stress:

A classic quantity in wall turbulence is the Reynolds stress, defined as $-\overline{u'w'}$, where the bar is a time average. Reynolds stress is a measure of the vertical flux of horizontal momentum. A negative value for $u'w'$ indicates a flux of positive horizontal momentum downward to be absorbed in the bottom boundary layer through the mechanism of bottom friction.

A tidal channel similar to that of Pickering Passage is that used by Gross and Nowell (1983) in Skagit Bay. They reported a value of $-u'$ that was 14% of the perturbation kinetic energy $u'^2 + v'^2 + w'^2$. The VM does not measure v', the spanwise or cross-stream perturbation velocities. It is assumed to be small compared to the streamwise and vertical components. The ratio of $-u'$ and q^2 is presented in Fig. 8. The mean value over the interval (smaller than shown) is 0.14, as was reported by Gross and Nowell (1983). This result might have been used as confirmation of performance, but that conclusion should be tested with analyses of additional observations.

4. Friction velocity and Reynolds stress:

Under conditions satisfied in the present situation, the mean velocity profile ($U(z)$) can be described as

$$U(z) - U_\infty = \frac{u_*}{\kappa} \ln(z/\delta)$$

where U_∞ is the free stream velocity, u_* is the friction velocity, κ is von Karman's constant (taken to be 0.4) and δ is the boundary layer thickness. Stress, τ, is related to u_* according to the

$$\tau = \rho u_*^2.$$

In a neutral, zero-pressure gradient, turbulent boundary layer, it is verified (e.g., Gross and Nowell, 1983) that $-\overline{u'w'} = u_*^2$. Friction velocity is determined with a fit to the mean horizontal velocity profile shown in Fig. 12. The slope is u_*/κ yielding a value over the interval from 1 to 10 m above the bottom of u_* of 0.05 m s^{-1}.

The Reynolds stress profile is shown in Fig. 13. The average value over the bottom 10 m is $1.7 \times 10^{-2} \text{ m s}^{-1}$, expressed in units of velocity (i.e., $(-\overline{u'w'})^{1/2}$).

Thus, in this data set the friction velocity is 2-3 times the square root of the Reynolds stress. Gross and Nowell (1983) reported that these quantities were about equal. One reason the friction velocity could be larger is because it represents the combination of friction and form drag which have acted over many eddy scales upstream, whereas the Reynolds stress represents only the local turbulent stress. This hypothesis could be tested by making numerous vertical profiles along an upstream track (as by reducing the length of the anchor line).

5. Eddy viscosity:

A balance between the Reynolds stress and mean shear requires

$$-\overline{u'w'} = \nu_e \frac{\partial U}{\partial z}.$$

where ν_e is the eddy viscosity. A comparison of $-\overline{u'w'}$ and U_z is shown in Fig. 14. The slope is about $2 \times 10^{-2} \text{ m}^2 \text{ s}^{-1}$, which is $200 \text{ cm}^2 \text{ s}^{-1}$. This value is comparable to values reported in
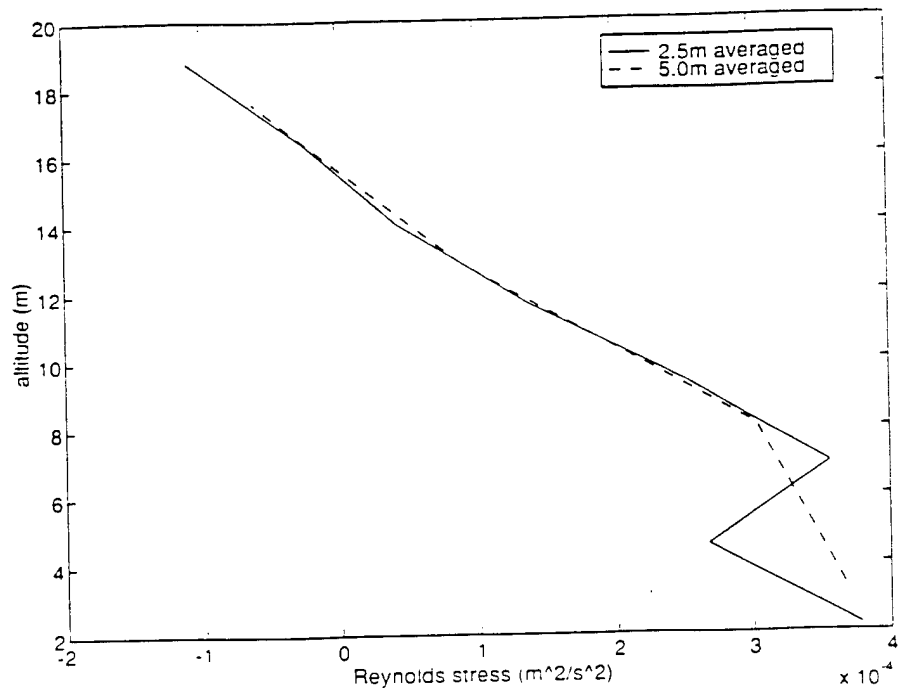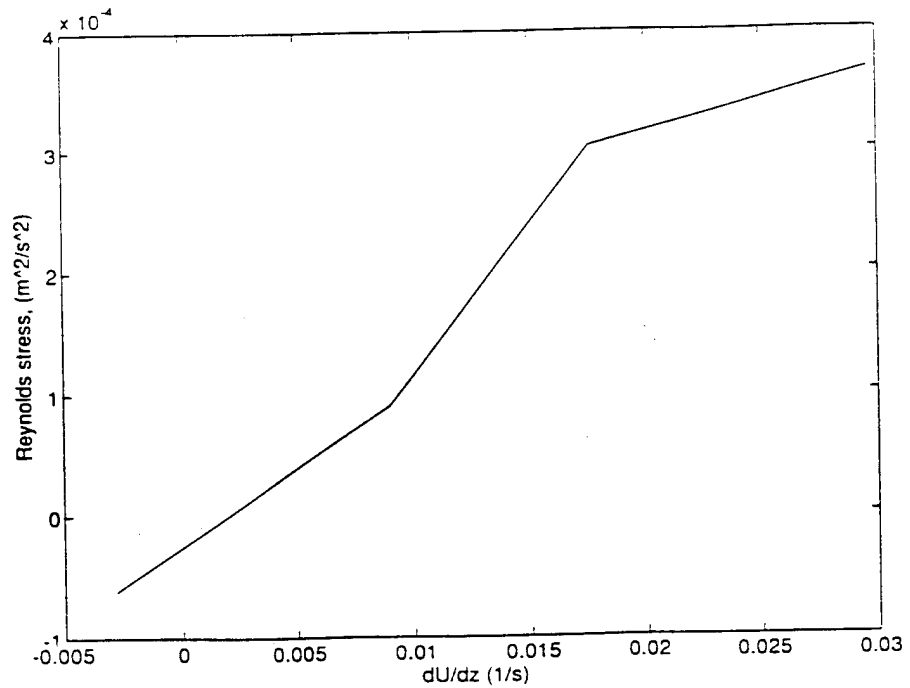
Figure 13. Reynolds stress vs. altitude.

Figure 14. Comparison between Reynolds stress and horizontal velocity shear. The observations nearest the bottom are in the upper right hand corner of the graph. The slope of the graph in the lower half of the water column is $2 \times 10^{-2} \, \mathrm{m^2 \, s^{-1}}$.

numerous coastal and tidal environments. The observations support a model consisting of a constant stress layer in which the eddy viscosity increases to a maximum value (here 2×10^{-2} m^{-2}s^{-1}) which remains approximately constant, at least until 15 m.a.b.

An estimate of the frictional sublayer thickness is ν/u_*. For a layer dominated by molecular viscosity the sublayer is very thin, less than 1 mm. The turbulent boundary layer is much thicker, more than a meter. A planetary boundary layer in a tidal channel is estimated by Bowden *et al.*, (1959) to be about $\pi \sqrt{2\nu_e/\omega}$ where ω is the tidal frequency (here the semi-diurnal tide). This boundary layer is more than 50 m when fully developed (and not constrained by the presence of the free surface).

6. Comparison of mean and perturbation KE:

Gross and Nowell (1983) reported that the ratio of perturbation and mean kinetic energies is about 2%. Computations were carried out on 1-Hz data after 4200 s by applying a 100-s box car, high-pass filter to obtain u' and a low-pass version of the same filter to get U. For a 750-s portion of the record while the VM was at an altitude of about 1 m, the ratio of the means is 2%. A time series of q^2/U^2 is shown in Fig. 15.

7. Vorticity and enstrophy (vorticity squared) versus altitude:

Much of the reason for making the observations was to learn about the magnitude and vertical distribution of vorticity. A comparison of vorticity versus mean vertical shear was presented earlier. They are equivalent determinations of the mean vorticity profile, and they are equal. In the context of instrument performance, this result is significant.

In analogy to the Reynolds stress formulation, one can derive an equivalent eddy transport equation for perturbation vorticity. It is of the form:

$$-\overline{w'\omega'} = K \frac{\partial \overline{\omega}}{\partial z}$$

where ω is the spanwise (horizontal) vorticity, $\overline{\omega}$ is the time-mean spanwise vorticity and K is an eddy diffusivity for vorticity. This balance has not been studied yet.

Figure 16 presents two forms of perturbation enstrophy. Both profiles of enstrophy are about equal and exhibit strong enhancement as the bottom is approached. The bottom 1 m may show a decrease from the enstrophy values just above. This may reveal the presence of that inner or constant (both viscous and eddy contributions) stress boundary layer often estimated as ν_e/u_* which is about 0.5 m. Another "rule of thumb" is that this layer is about 6% of the water column or here about 1 m. Thus, the behavior of enstrophy and other variables within 1 m of the bottom should be different than that immediately above, out of the inner layer.

What governs the height variation of enstrophy if not u_* and z? Stratification and buoyancy flux terms are too small to matter. It should be remembered that the analysis concentrated on 1-Hz data; it is possible that the 20-Hz observations will exhibit different behavior. Time variation could be important in that the flow is changing during the analysis interval. If enstrophy is being generated only at the bottom and is transported vertically, the amount may be larger than expected at a given height during a decelerating flow and smaller during an accelerating tide. This hypothesis could be tested with this and future data sets.

9. Discussion:

This very preliminary study of portions of a larger data set has demonstrated satisfactory performance for the VM system and confirmed some classic boundary layer results.
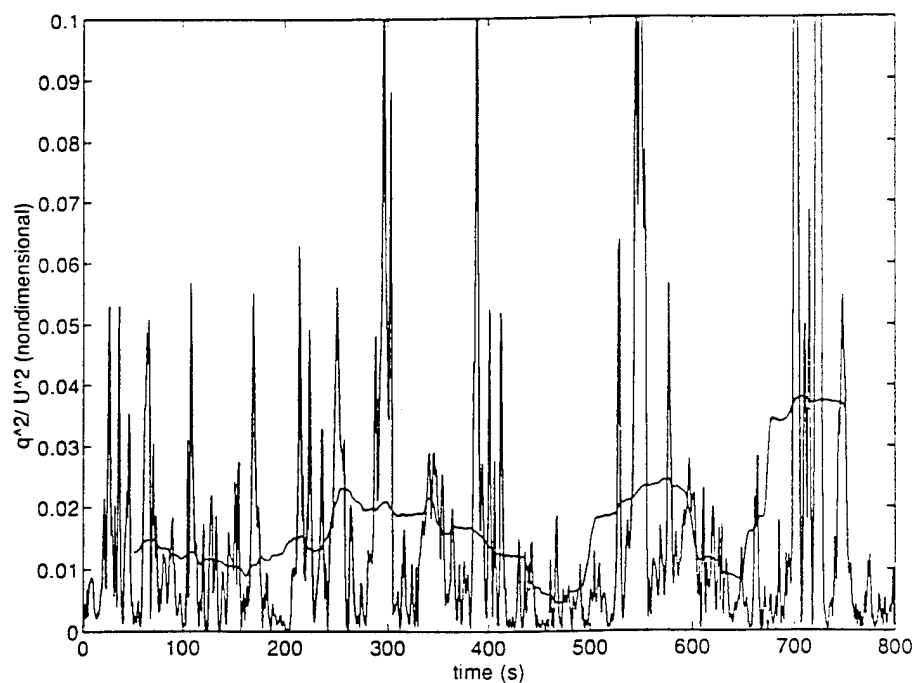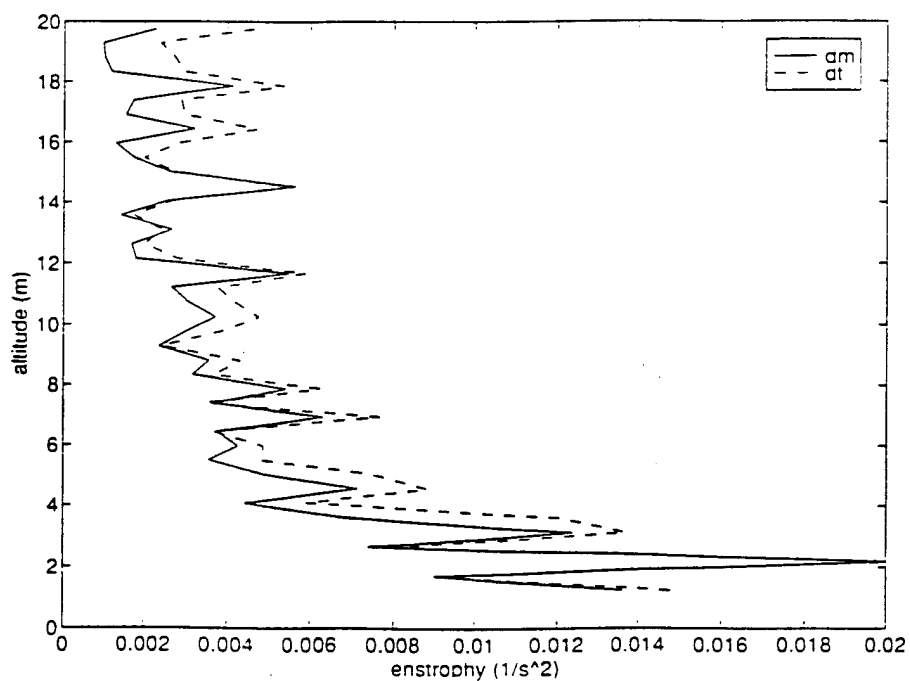
Figure 15. Time series of $\dfrac{q^2}{U^2}$.

Figure 16. Comparison of enstrophy values using vorAadm and vorAadt, two versions of high-passed vorticity.

It appears that there are three regions in these data. At the lowest level, below about 1 m, the structure exhibits characteristics of an inner layer where molecular and eddy viscosities are both important. Between 1.5 and 10 -15 m.a.b. there is an outer layer with a well formed log layer in mean velocity. Above 15 m.a.b. there is another layer where the presence of the free surface restricts the growth of eddies and where wind forcing and air-sea interactions, such as buoyancy fluxes, contribute additional influences. This structure is consistent with the models discussed by Gross (1986).

The mean velocity and mean vorticity are consistent with a classic turbulent log layer. A value of u_* of 5.0×10^{-2} m s^{-1} was found over the bottom 10 m.

The eddy contributions and statistics also exhibit "law of the wall" characteristics and are comparable to previous investigations. In particular, we find that $-\overline{u'w'}/q^2$ is 13%, comparable to the 14% reported by Gross and Nowell (1983) in a similar tidal channel. The ratio of Reynolds stress to mean vertical shear was about constant in the lower 10 m with a value of about 2×10^{-2} m^{2}s^{-1}. This estimation of an eddy viscosity is comparable to other determinations in comparable settings.

The perturbation vorticity and enstrophy observations are unique in this study. The behavior of spanwise vorticity was a puzzle at first. Simple dimensional arguments predicted a height dependence of u_*/z. That is, perturbation vorticity decreasing as inverse height above the bottom. Clearly, the dependence is more like the inverse square root of height. This behavior can be understood in terms of the dynamics of the constant stress layer. The balance of production and dissipation requires that

$$\varepsilon = -\overline{u'w'}\frac{\partial U}{\partial z}. \tag{1}$$

But $-\overline{u'w'} = u_*^2$ and the mean vertical shear is $u_*/\kappa z$. Hence,

$$\varepsilon = \frac{u_*^3}{\kappa}z.$$

The fundamental definition of ε used in microstructure studies is

$$\varepsilon = \frac{15}{2}\nu\int_0^\infty k^2\phi\,dk = \frac{15}{2}\nu\overline{\frac{\partial u}{\partial z}^2}.$$

where $\phi(k)$ is the one-dimensional kinetic energy density function and k is the one-dimensional wavenumber. The definition of ϕ is

$$\int_0^\infty \phi(k)\,dk = \frac{1}{2}\overline{u^2}.$$

In isotropic turbulence,

$$\overline{(\frac{\partial u}{\partial z})^2} = \frac{1}{2}\overline{\omega_y^2}.$$

In terms of a single component of vorticity, the kinetic energy dissipation is

$$\varepsilon = \frac{15}{4}\nu\overline{\omega_y^2}.$$

The one-dimensional vorticity can be expressed in terms of a one-dimensional vorticity variance

or enstrophy spectral function:

$$\int_0^\infty \psi(k)\,dk = \overline{\omega_y^2}.$$

We do not resolve the total vorticity spectrum. Wyngaard showed that it is necessary to measure vorticity down to length scales that are less than 3 times the Kolmogorov microscale, $(\nu^3/\varepsilon)^{1/4}$. We do not achieve this millimeter scale, so our estimate of enstrophy is deficient at the high wavenumber end, namely,

$$\overline{\omega_y^2} = \int_0^{k_s} \psi(k)\,dk\;.$$

where k_s is the cut-off wavenumber of the VM, about 60 m^{-1} (10 cpm). There is some reason to expect that the missing variance is proportional to that which is resolved. To see this, suppose the measurements are in the inertia subrange characterized by a velocity spectrum proportional to $k^{-5/3}$. The vorticity spectrum is nearly flat with a slope of $k^{1/3}$. If the spectrum were flat, the resolved variance would be of order k_s/η^{-1}, where η is the Kolmogorov microscale. The resolved vorticity variance by the VM is less than 10% of the total variance.

This argument leads one to boldly suggest that the level of vorticity variance in the middle of the inertial subrange may be indicative of vorticity variance at the dissipation scale. In this case we formulate a macroscale relation of the form:

$$\varepsilon = C\nu_e \overline{\omega_y^2} \tag{2}$$

where C is an order unity constant and ν_e is the eddy viscosity. The equality of the two ε determinations (i.e., (1) and (2)) yields:

$$\overline{\omega_y^2} = \frac{u_*^3}{C k \nu_e z}\;.$$

One notable aspect of this formulation is that it explains the inverse height dependence for enstrophy. Another is that it provides an estimate of signal levels for comparison with laboratory vorticity measurements. For example, Balint *et al.* (1991) reported vorticity determinations in a wind tunnel using hot wire anemometers configured to measure vorticity components. They applied an outer scaling for vorticity, namely a normalization by u_*/δ, where δ is the boundary layer thickness. This factor amounts to a factor of 800 for a δ of 50 m and u_* of 0.05 m s^{-1}. Hence, the normalized spanwise rms vorticity is

$$\frac{\omega_z \delta}{u_*} = (\frac{u_* \delta}{C k \nu_e})^{\frac{1}{2}} (\frac{z}{\delta})^{-\frac{1}{2}}. \tag{3}$$

For the brief series under study here the quantities are $u_* = 0.05$ m s^{-1}, $\delta = 50$ m, $C = \kappa$ (a guess), $\kappa = 0.4$ and $\nu_e = 2 \times 10^{-2}$ m^2 s^{-1}. The amplitude in the above equation is 28 (nondimensional).

The culmination of the present studies is the comparison of our tidal BBL observations with the only known comparison set, namely, a study of a wind-tunnel boundary by Balint *et al.* (1991). Figure 17 shows the comparison of these two very different experiments plotted in terms of outer-layer scaled variables. The agreement is very good; a result that was not expected *a priori*. Moreover, the prediction of (3) is plotted along with the observations. The two

observations and the prediction agree in amplitude and vertical dependence. The function in (3), the observations of Balint *et al.* (1991) and our tidal channel observations are plotted in Fig. 17.

The results are very gratifying. The velocity measurements confirm expectations from previous measurements and modeling to tidal channels. The vorticity and enstrophy observations behave about as expected. That is, mean vorticity was expected to agree with mean vertical shear and perturbation enstrophy exhibited a monotonic increase toward the bottom (except in the bottom 1 m or so where it decreased). The ratio of rms streamwise velocity and rms spanwise vorticity increased with altitude, consistent with the dominant and energetic eddies growing in scale. The increase was not linear as expected the from the mixing length argument but was proportional to the square root of height. Further conclusions should wait until more of the observations are analyzed. In particular, more attentions should be given to the 20-Hz data. Also, performance evaluations should continue.
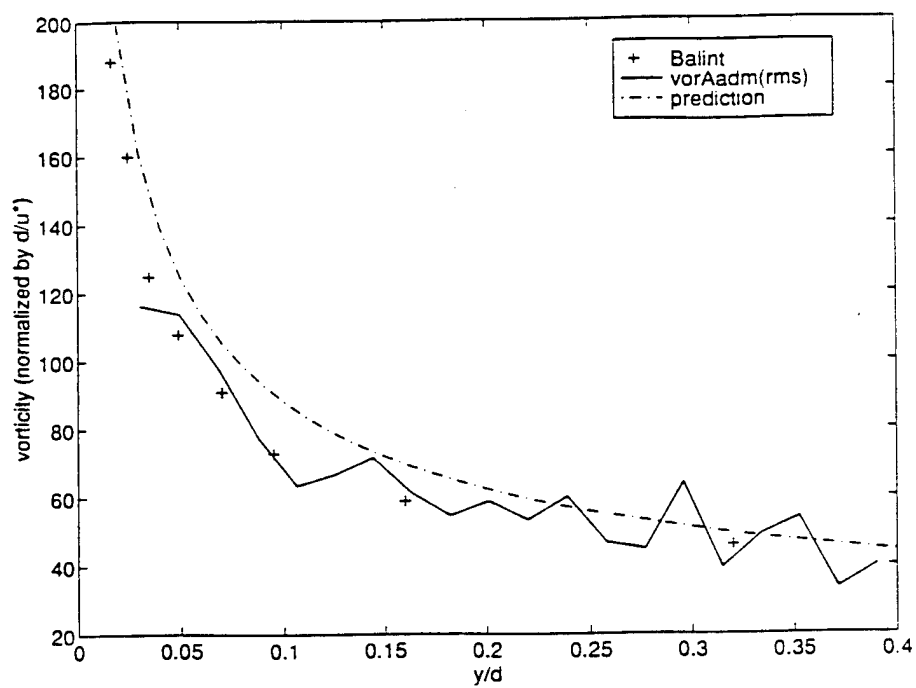
Figure 17. Comparison of BBL scaled spanwise vorticity from measurements of Balint *et al.* (1991), the VM and from relation derived in text.